PHYSICAL REVIEW A VOLUME 28, NUMBER 5 NOVEMBER 1983

Orbital collapse and the photoionization of the inner 4*d* shells for Xe-like ions

K. T. Cheng
Argonne National Laboratory, Argonne, Illinois 60439

W. R. Johnson
Physics Department, University of Notre Dame, Notre Dame, Indiana 46556
(Received 27 September 1982; revised manuscript received 23 May 1983)

Photoionization of the inner 4*d* shells for Xe, Cs^+, Ba^{2+}, and La^{3+} are studied with the use of the relativistic random-phase approximation. Total cross sections, partial cross-section branching ratios, and angular-distribution asymmetry parameters are calculated, and their systematic trends along the isoelectronic sequence are studied. Important dynamic effects of electron correlations are obtained from an eigenchannel analysis involving the eigenquantum defects, the eigendipole amplitudes, and the transformation U matrices. We find that there are shape resonances in the effective potential for f electrons, and that the collapse of the 4*f* orbital along the isoelectronic sequence is closely related to changes in f orbitals in passing through these resonances.

I. INTRODUCTION

The photoionization of the inner 4*d* shells for Xe is known to have a giant resonancelike structure in the cross section which peaks at about 25 eV above the 4*d* thresholds and extends over a range of about 60 eV.[1] This delayed onset of photoionization can be understood qualitatively in terms of the effective potential for f orbitals which has a two-well structure—an inner well separated from the outer one by a potential barrier.[2] At low energy, f orbitals are kept away from the inner well by the potential barrier so that there are very little overlap with the 4*d* wave functions. As a result, the cross section near the ionization threshold is small, and the autoionization resonances arising from the $4d \rightarrow nf$ discrete excitations are weak. As the energy increases, however, f orbitals gradually surmount the potential barrier and eventually contract into the inner well. This leads to dramatic increases in the transition amplitudes of the $4d \rightarrow f$ channels and hence the resonancelike structure in the cross section.

Along the isoelectronic sequence, the inner well becomes deeper and deeper as nuclear charge increases. At some point, the inner well is deep enough to support a bound state of its own, and the 4*f* orbital is suddenly "collapsed" into the inner well. Possible consequences of the 4*f* orbital collapse are studied in a recent experiment on the absorption spectra of Ba, Ba^+, and Ba^{2+} by Lucatorto *et al.*[3] In this experiment, it was found that the spectra of Ba and Ba^+ are similar to that of neutral Xe, with resonancelike structure above the 4*d* thresholds and weak resonance lines below them. The spectrum of Ba^{2+}, on the other hand, is entirely different. The cross section now starts from a sizable value (~ 30 Mb) at the thresholds, and decreases monotonically afterwards. At the same time, strong resonance lines appear in the discrete excitation region.

While these sudden changes in the spectra appear to result from orbital collapse occurring in Ba^{2+}, the interpretation of these observations was not very clear. According to earlier discussions of the collapse phenomenon in rare-earth atoms,[4,5] even after the 4*f* orbital is collapsed, transitions to higher nf levels ($n \geq 5$) remain suppressed by the potential barrier. As a result, in the words of Lucatorto *et al.*, "one would have expected only one strong line that associated with the $4d^9 4f\,{}^1P$, and not four lines as observed." Based on a configuration-average Hartree-Fock (HF) model, they showed that the $4d^9 4f\,{}^1P$ level is below the ionization threshold, and interpreted the Ba^{2+} spectrum as due to the partial collapse of the 4*f* orbital. On the other hand, a more recent paper by Connerade and Mansfield[6] suggested that the observed lines are associated with the $4d \rightarrow 5f, 6f, \ldots$ transitions rather than with the $4d \rightarrow 4f$ excitation, and that because of orbital collapse, the $4d^9 4f\,{}^1P$ level actually lies above the 4*d* thresholds, leading to the large absorption cross section at the onset of photoionization.

Part of the confusion about the collapse of the 4*f* orbital and the position of the $4d^9 4f\,{}^1P$ level arises from the fact that these discussions are based on rather simple atomic models. An example is given in Ref. 7 where the position of the $4d^9 4f\,{}^1P$ level in Ba atom was shown to be very model dependent. A more detailed discussion of orbital collapse and the influence on the $4d \rightarrow nf$ discrete spectra of Xe-like ions is given elsewhere.[8]

In this work, we shall concentrate on the part of the spectra above the 4*d* ionization limits for Xe, Cs^+, Ba^{2+}, and La^{3+}. Unlike the experiment of Lucatorto *et al.*, we are studying along the Ba^{2+} isoelectronic sequence rather than along its isonuclear sequence because in this way, systematic trends in the photoelectron spectra are not complicated by the change in the electronic configuration. For a quantitative understanding of the photoionization of the inner 4*d* shells for Xe-like ions, we employ the relativistic random-phase approximation (RRPA) to account for the relativistic and electron correlation effects. We find that the spectra are strongly term dependent and are very sensitive to correlation effects. Also, there are shape resonances in the effective potential for f electrons. They

are actually eigenstates of the inner potential well. As the inner well deepens along the isoelectronic sequence, these shape resonances gradually move down into the discrete excitation region, interact with all nf levels, and eventually lead to the collapse of the $4f$ orbital when they come below the entire Rydberg series. Detailed discussions of these phenomena and their physical implications will be given in Secs. III and IV. In Sec. II we shall first describe the theoretical technique in calculating and analyzing the results.

II. THEORY

The RRPA is an approximated relativistic many-body theory designed to study the response of an atom to an external field. Detailed discussions of this theory applied to photoexcitation and photoionization processes have been given before.[9,10] The dynamics of these processes are described by a set of coupled-channel radial equations for the perturbed orbitals $y_i(r)$ as

$$[h+V_i-(\epsilon_i\pm\omega)]y_{i\pm}(r)=\sum_j V_{ij}^{(\pm)}y_{j\pm}(r)\ , \tag{1}$$

where h is the single-particle Hamiltonian, V_i is the HF potential operator, ϵ_i is the eigenenergy of the unperturbed HF orbital $u_i(r)$, ω is the frequency of the external photon field, and V_{ij} is the channel-coupling potential operator. Here $\pm$ refers to the positive- and negative-frequency excitation channels, respectively, and atomic units are used throughout this paper. For a set of N coupled-channel RRPA equations, let there be M open channels ($M\le N$) that lead to direct ionization and let the rest be closed channels, we can construct M sets of independent coupled-channel solutions to Eq. (1) that are regular at the origin and that satisfy the asymptotic boundary conditions

$$y_j^{(i)}(r)\rightarrow f_j(r)\delta_{ji}+g_j(r)R_{ji}\ ,\quad i,j=1,2,\ldots,M\ . \tag{2}$$

Here $y_j^{(i)}(r)$ refers to the perturbed orbital $y_j(r)$ in the ith coupled-channel solution, $f_j(r)$ and $g_j(r)$ are the regular and irregular Coulomb wave functions as defined in Eqs. (74) and (75) of Ref. 9, and R_{ji} is the reactance matrix. In Eq. (2), $y_j^{(i)}(r)$ refers to open-channel positive-frequency orbitals only. Closed-channel orbitals as well as all negative-frequency orbitals vanish exponentially at large r and are not shown here. From these RRPA solutions, the dipole transition amplitude for the ith open channel is given by

$$D^{(i)}=\sum_{j=1}^{N}(\langle y_{j+}^{(i)}||Q||u_j\rangle+\langle y_{j-}^{(i)}||Q||u_j\rangle)\ , \tag{3}$$

where $\langle y_j||Q||u_j\rangle$ is the reduced matrix element of the dipole operator Q.

The reactance matrix R_{ji} defined in Eq. (2) is real and symmetric.[9] Let $U_{i\alpha}$ be the matrix of eigenvectors of R_{ji}, then $U_{i\alpha}$ is an orthogonal matrix which diagonalizes R_{ji}, with real eigenvalues $\lambda_\alpha=\tan(\pi\mu_\alpha)$, $\alpha=1,2,\ldots,M$. The eigenchannel solutions $z_j^{(\alpha)}$ are standing-wave solutions obtained from particular linear combinations of $y_j^{(i)}(r)$ as

$$z_j^{(\alpha)}(r)=\sum_{i=1}^{M}y_j^{(i)}(r)U_{i\alpha}\cos(\pi\mu_\alpha)$$
$$\rightarrow[f_j(r)\cos(\pi\mu_\alpha)+g_j(r)\sin(\pi\mu_\alpha)]U_{j\alpha}\ ,$$
$$j,\alpha=1,2,\ldots,M\ . \tag{4}$$

Thus $\pi\mu_\alpha$ as defined by the eigenvalue λ_α is the common non-Coulomb phase shift for all orbitals in the αth eigenchannel solution, with μ_α being the eigenquantum defect. Corresponding eigendipole amplitudes D_α for the transitions to these eigenchannels are given by

$$D_\alpha=\sum_{i=1}^{M}D^{(i)}U_{i\alpha}\cos(\pi\mu_\alpha)\ ,\quad \alpha=1,2,\ldots,M\ . \tag{5}$$

Eigenchannel solutions are important because the channel coupling terms in Eq. (1) are diagonalized by these solutions, with the equations for $z_j^{(\alpha)}(r)$ being completely decoupled. As a result, the eigenchannel data μ_α, D_α, and $U_{i\alpha}$ are usually slowly varying functions of energy, and contain important information on the dynamics of electron-electron interactions in photoexcitation processes. Furthermore, according to the multichannel quantum-defect theory (MQDT),[11–13] these parameters can be continued smoothly below the ionization threshold into the autoionization and the discrete excitation region. Since physically acceptable solutions to the coupled-channel equation (1) are superpositions of eigenchannel orbitals subjected to proper physical boundary conditions, the whole spectrum including the discrete, autoionization, and continuum regions is thus determined completely by these eigenchannel data. In the continuum spectrum, for example, the "incoming wave" boundary condition dictates that physical transition amplitudes are given by the eigenchannel data as[9,12]

$$\bar{D}_i=\sum_{\alpha=1}^{M}D_\alpha U_{i\alpha}e^{-i\pi\mu_\alpha}\ ,\quad i=1,2,\ldots,M\ , \tag{6}$$

and from these amplitudes, all physical observables such as cross sections and photoelectron angular distributions and spin polarizations can be determined. For example, subshell cross section σ is given by

$$\sigma=\tfrac{4}{3}\pi^2\alpha\omega\sum_i|\bar{D}_i|^2\ , \tag{7}$$

where α is the fine-structure constant, and where the summation includes all channels that originate from the same subshell. The differential cross section is then given by

$$\frac{d\sigma}{d\Omega}=\frac{\sigma}{4\pi}\left[1-\frac{\beta}{2}P_2(\cos\theta)\right] \tag{8}$$

with β being the angular distribution asymmetry parameter determined completely by the transition amplitudes $\bar{D}_i$ and θ being the angle between the incident photon and the outgoing electron. In the following sections, we shall demonstrate what one can learn from these eigenchannel data about the term dependence and correlation effects in the $4d$ photoionizations for Xe-like ions and, in particular, about the collapse of the $4f$ orbital.

III. RESULTS AND DISCUSSIONS

A. Cross sections and angular distributions

In our studies of the photoionization of inner $4d$ shells for Xe, Cs^+, Ba^{2+}, and La^{3+}, we include six interacting channels in the RRPA calculations: They are the $4d_{3/2} \rightarrow p_{1/2}, p_{3/2}, f_{5/2}$ and $4d_{5/2} \rightarrow p_{3/2}, f_{5/2}, f_{7/2}$. Correlation effects arising from the outer $5s$ and $5p$ shells and from other inner shells are weak and are neglected. Also, only length form results are presented here, as length and velocity form transition amplitudes are very close to each other in RRPA studies.[9,10] Results of our calculations on the photoionization cross sections of these Xe-like ions are shown in Fig. 1 as functions of photon energy. Except for the shift in the ionization thresholds, these cross sections actually resemble each other, and follow closely the structure laid out by that of neutral Xe. In particular, as the thresholds of Xe and Cs^+ are at lower energy, there are peaks in their cross sections near 100 eV. On the other hand, Ba^{2+} and La^{3+} have higher $4d$ ionization limits, and their cross sections simply decrease monotonically after the onsets of photoionizations. Regardless of their threshold positions, all these cross sections go through their respective Cooper minima near 190 eV before they increase again.

In Fig. 2, we compare our results on the cross sections of Xe and Ba^{2+} with experiment and with other theories. The Xe cross section has been studied in detail before. In a Herman-Skillman (HS) potential calculation,[14] the theoretical cross section was found to peak too high and to come too close to the ionization thresholds. Good agreement with experiment can be attained only by including HF exchanges[15,16] and electron correlations[17] in the calculation, thereby broadening and shifting the cross-section peak to higher energy. Our RRPA results are in good agreement with those of the nonrelativistic random-phase approximation with exchange (RPAE),[17] indicating that spin-orbit effects are not important for cross sections. Along the isoelectronic sequence, the Ba^{2+} cross section has been studied in the HF approximation with and without the inclusion of relaxation effects.[18] It is interesting to note that the correlated RRPA results are in very good agreement with the unrelaxed HF results which are geometric means of length and velocity form values.

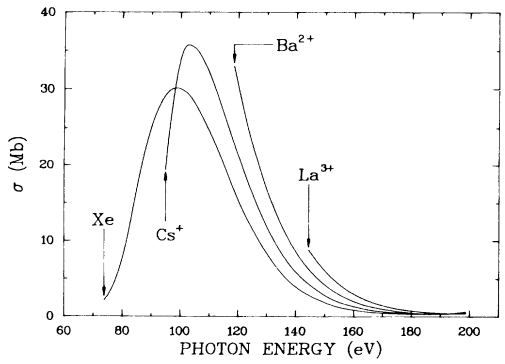

FIG. 1. Photoionization cross sections for Xe, Cs^+, Ba^{2+}, and La^{3+} as functions of photon energy.

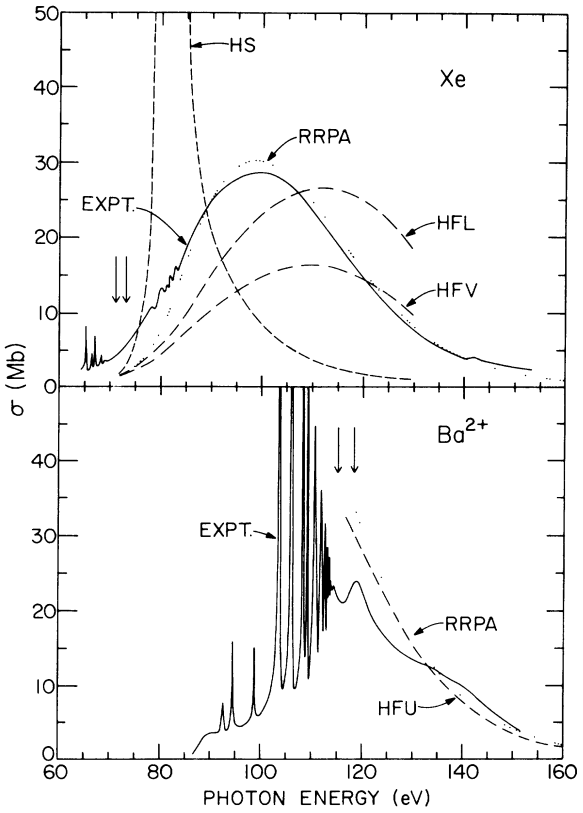

FIG. 2. Comparison between theory and experiment on the absorption cross sections of Xe and Ba^{2+}. Arrows show the ^2D thresholds of these ions. Upper graph, Xe. Experiment: ——, Haensel *et al.*, Ref. 1. Theory: · · ·, RRPA, this work; —·—, HF length (HFL) and velocity (HFV) form results of Starace, Ref. 15; — — —, Herman-Skillman (HS) potential results of Starace, Ref. 15. Lower graph, Ba^{2+}. Experiment: ——, Lucatorto *et al.*, Ref. 3. Theory: · · ·, RRPA, this work; —·—, unrelaxed HF (HFU) results of Kelly *et al.*, Ref. 18.

In Fig. 1, it appears that there is a rather simple trend in the absorption spectra of Xe-like ions above the $4d$ thresholds: The general features of these spectra are basically the same along the isoelectronic sequence except for a gradual shift of the cross sections towards higher photon energy as nuclear charge Z increases. This is consistent with a comparison of the experimental absorption spectra of solid KI, Xe, and CsCl in the energy range of 50—140 eV where their cross sections are dominated by the atomic $4d \rightarrow f$ transitions for I^- ions, Xe, and Cs^+ ions, respectively.[19] If this trend continues, the $4d$ thresholds of Ce^{4+} and Pr^{5+} should be very close to the Cooper minima near 190 eV. As a result, one would expect the cross sections of these two ions to start from small values at the thresholds and to go up at higher energy.

Of course, similar trends have been found in the photoionization cross sections of outer np shells for ions in rare-gas isoelectronic sequences.[20] We find, however, that other physical observables also seem to follow the same trend as the cross sections. In Figs. 3 and 4, the partial

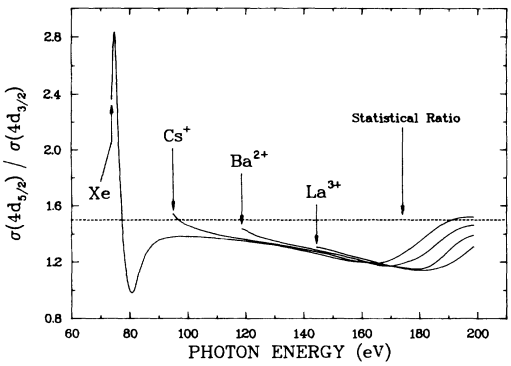

FIG. 3. $4d_{5/2}$ to $4d_{3/2}$ branching ratios for Xe, Cs^+, Ba^{2+}, and La^{3+} as functions of photon energy.

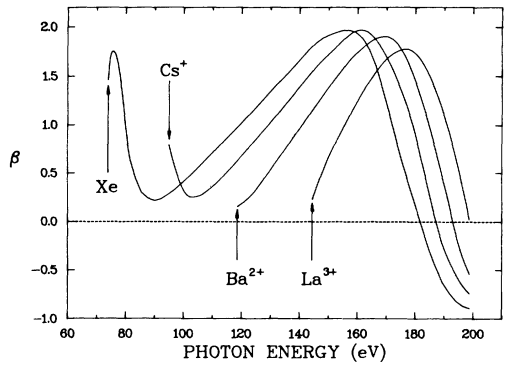

FIG. 4. Average angular distribution asymmetry parameters for the $4d$ photoelectrons of Xe, Cs^+, Ba^{2+}, and La^{3+} as functions of photon energy.

cross-section branching ratios of the $4d_{5/2}$ and $4d_{3/2}$ subshells and the average angular-distribution asymmetry parameters β for the $4d$ photoelectrons are shown as functions of photon energy. Comparing Figs. 1, 3, and 4, the similarity in the systematic trends is certainly unmistakable. Detailed RRPA studies of the Xe photoionization spectrum including cross sections, angular distributions, and spin polarizations have been given before.[21] Comparisons with experiment and with other theories have been reported for the branching ratio,[22] and the angular distribution asymmetry parameter.[23] In general, there are excellent agreements between theory and experiment on the Xe spectrum. Unfortunately, no study is presently available for any other Xe-like ions for similar comparisons.

B. Eigenchannel data

To make a more detailed analysis of the systematic trends of photoelectron spectra, and to understand the dynamics of $4d$ photoionization processes, we turn our attention to the eigenchannel data μ_α, D_α, and $U_{i\alpha}$, as they determine the spectra completely. Since the eigenchannels are in general closer to the LS- than to the jj-coupling schemes, they are labeled by their approximated LS designations: $(d^9f)\ ^1P,^3P,^3D$ and $(d^9p)\ ^1P,^3P,^3D$. The matrix $U_{i\alpha}$ is the transformation matrix that connects the jj-coupled channels labeled by the indices "i" to the eigenchannels labeled by the indices "α." The assignments of these indices are given as follows:

$i,\alpha=$	1	2	3	4	5	6
i	$4d_{5/2}p_{3/2}$	$4d_{5/2}f_{5/2}$	$4d_{5/2}f_{7/2}$	$4d_{3/2}p_{1/2}$	$4d_{3/2}p_{3/2}$	$4d_{3/2}f_{5/2}$
α	$(d^9f)\ ^3P$	$(d^9f)\ ^3D$	$(d^9f)\ ^1P$	$(d^9p)\ ^3D$	$(d^9p)\ ^3P$	$(d^9p)\ ^1P$

The RRPA eigenquantum defects μ_α and eigendipole amplitudes D_α for Xe, Cs^+, Ba^{2+}, and La^{3+} are shown as functions of photon energy in Figs. 5 and 6, respectively. Again, like the cross section and other physical observables shown in Figs. 1, 3, and 4, these parameters are rather insensitive to the increase in nuclear charge, and their general features remain the same along the isoelectronic sequence. A similar trend is also found in the U matrix. We present, in Table I, numerical values of these matrices for Xe, Cs^+, Ba^{2+}, and La^{3+} at their respective $^2D_{3/2}$ thresholds. Changes in these matrices thus reflect their energy dependence. For comparison purposes, the transformation matrix that connects the jj-coupled channels to the exact LS-coupled channels is given in Table II. In the LS-coupling limit, the U matrix should be identical to this jj-LS transformation matrix, while in the jj-coupling limit, it should simply be the identity matrix.

In Fig. 5, one notices that μ_α are divided into two groups: One corresponds to the $4d\rightarrow f$ channels ($\alpha=1,2,3$) and the other to the $4d\rightarrow p$ channels ($\alpha=4,5,6$). Like the jj-LS transformation matrix, the U matrices in Table I are nearly block diagonal, indicating weak interactions between the $4d\rightarrow f$ and the $4d\rightarrow p$ channels. In Fig. 5, the eigenquantum defects μ_α of the $4d\rightarrow p$ channels remain very close to each other, and decrease slowly as photon energy increases. Furthermore, for a given photon energy, their values decrease monotonically with increasing Z, indicating the approach towards the hydrogenic limit along the isoelectronic sequence. In Fig. 6, the eigendipole amplitudes D_α of the $4d\rightarrow p$ channels also remain very close to each other and vary slowly with photon energy. An interesting feature here is that these amplitudes are all comparable in size and that the two triplet transition amplitudes are not at all suppressed. This shows that the eigenchannels of the $4d\rightarrow p$ transitions are not very close to the LS-coupling scheme. Inspection of the U matrices in Table I clearly supported this observation.

While the $4d\rightarrow p$ channels have rather simple features, the spectra are nevertheless dominated by the $4d\rightarrow f$ channels with quite different behavior. In Fig. 5, one sees that the three μ_α of the $4d\rightarrow f$ channels ($\alpha=1,2,3$) are, in

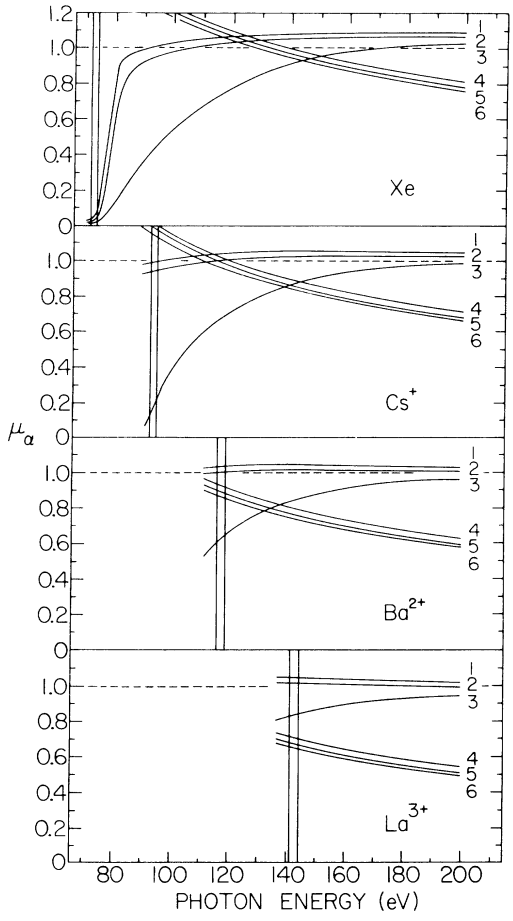

FIG. 5. Eigenquantum defects μ_α for Xe, Cs^+, Ba^{2+}, and La^{3+} as functions of photon energy. Vertical lines show the positions of the ^2D thresholds of these ions.

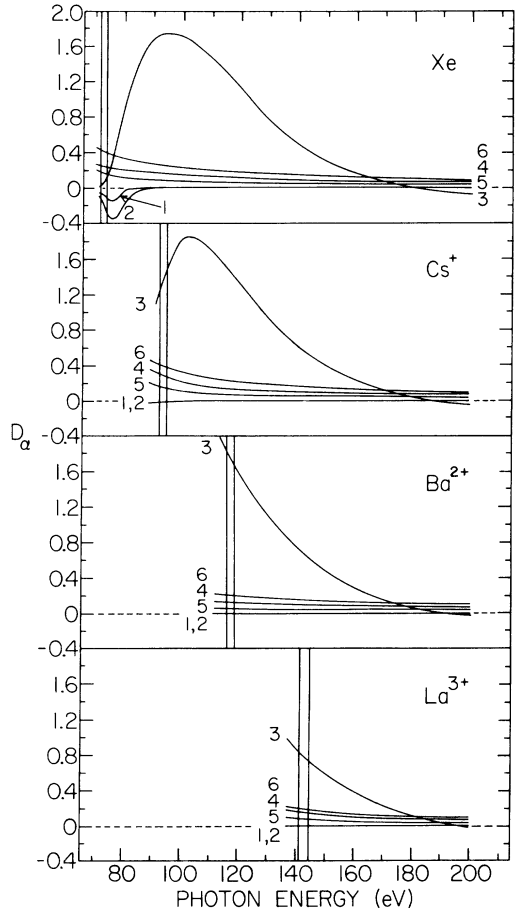

FIG. 6. Eigendipole amplitudes D_α for Xe, Cs^+, Ba^{2+}, and La^{3+} as functions of photon energy. Vertical lines show the positions of the ^2D thresholds of these ions.

general, not very close to each other in this energy range, and that they appear to divide into two groups: One consists of μ_1 and μ_2 of the ^3P and ^3D transitions, respectively, while the other consists of μ_3 of the ^1P transition only. Closer inspection of the Xe data in Fig. 5 shows that these μ_α all start from very small values near the $4d$ thresholds and increase rapidly with photon energy until their sizes change by about one. In this respect, these two groups of μ_α actually behave similarly, and their main difference is in their rates of changes with photon energy. Corresponding D_α in Fig. 6 show that the amplitudes of the ^1P channel ($\alpha=3$) are indeed very strong and that those of the ^3P and ^3D channels ($\alpha=1,2$) nearly vanish, except at low energy near the thresholds of Xe. In particular, the Cooper minima in the cross sections of these ions actually arise from the ^1P amplitudes which go through sign changes near 190 eV.

Comparing the U matrices of Cs^+, Ba^{2+}, and La^{3+} in Table I with the jj-LS transformation matrix in Table II, we find that the $4d\rightarrow f$ channels are indeed very close to the LS-coupling scheme at higher energy so that the triplet channels are suppressed while the singlet channel dominates the spectrum. At lower energy, however, the U matrix of Xe shows that the $4d_{3/2}\rightarrow f_{5/2}$ channel is nearly decoupled from the $4d_{5/2}\rightarrow f_{5/2},f_{7/2}$ channels. As a result, the eigenchannels are no longer well described by the LS-coupling scheme, and the amplitudes D_α of all three $4d\rightarrow f$ channels become comparable in size.

In Fig. 6, one sees that there is a huge peak in the ^1P amplitude extending well over 60 eV above the $4d$ thresholds of Xe, and that there are much weaker peaks in the ^3P and ^3D amplitudes with widths of about 10 eV only. The small peaks in the triplet amplitudes actually result from coupling changes where the jj-allowed $4d_{5/2}\rightarrow f_{5/2},f_{7/2}$ transitions gradually turn into the LS-forbidden $4d\rightarrow f$ $^3P,^3D$ excitations. The effect of this coupling change may not show up in the total cross section, which is dominated by the ^1P amplitude, but it does lead to a rapid variation in the cross-section branching ratio right above the $4d$ thresholds of Xe. The situation is clearly shown in Fig. 3. A more detailed comparison of the Xe branching ratio with experiment and with the Dirac-Fock (DF) results[24] is given in Fig. 7. One sees that the RRPA results are in very good agreement with experiment, especially near the threshold where they both go through rapid variations. The DF results, on the other

TABLE I. Transformation matrices $U_{i\alpha}$ for Xe, Cs^+, Ba^{2+}, and La^{3+} at their respective $^2D_{3/2}$ thresholds.

Ion	i/α	1	2	3	4	5	6
Xe	3	−0.513	−0.852	0.108	0.001	0.008	0.018
	2	0.853	−0.520	−0.052	0.015	−0.003	−0.004
	6	0.101	0.066	0.993	0.006	0.001	0.003
	1	0.016	0.012	−0.004	−0.197	0.139	0.970
	5	0.010	−0.005	0.003	−0.637	0.734	−0.235
	4	−0.004	0.010	−0.005	0.745	0.664	0.056
Cs^+	3	−0.514	−0.400	0.738	−0.127	−0.069	−0.103
	2	0.738	−0.657	0.147	−0.041	−0.024	−0.010
	6	0.437	0.639	0.615	−0.111	−0.039	−0.095
	1	−0.006	0.009	0.113	−0.231	0.239	0.936
	5	−0.006	−0.016	−0.059	−0.461	0.826	−0.317
	4	0.011	−0.015	0.200	0.839	0.503	0.055
Ba^{2+}	3	−0.526	−0.393	0.751	−0.033	−0.024	−0.045
	2	0.732	−0.661	0.166	0.002	0.010	−0.015
	6	0.433	0.639	0.633	−0.045	−0.030	−0.028
	1	−0.004	−0.006	0.054	−0.165	0.358	0.917
	5	−0.005	0.012	−0.010	−0.359	0.846	−0.394
	4	−0.002	0.022	0.063	0.917	0.393	0.008
La^{3+}	3	−0.552	−0.353	0.755	0.019	0.003	−0.013
	2	0.696	−0.694	0.185	0.001	0.009	−0.003
	6	0.459	0.628	0.629	0.009	0.007	−0.008
	1	−0.005	−0.001	0.013	−0.140	0.410	0.901
	5	−0.008	0.002	−0.008	−0.298	0.850	−0.433
	4	0.003	0.003	−0.022	0.944	0.330	−0.003

hand, deviate substantially from experiment. This shows once again the importance of correlation effects in low-energy photoionization.

C. Autoionization resonances

From the systematic trends in cross sections and various other data shown above, it is obvious that changes in the spectra along the isoelectronic sequence can be understood qualitatively in terms of the spectrum of neutral Xe. For example, the threshold value of the cross sections as a function of Z can be estimated simply from the Xe cross section at the respective threshold energies of the stripped ions. But perhaps the most interesting consequence of all is that general properties of the discrete spectrum can be likewise determined. According to MQDT,[11–13] discrete, autoionization and continuum spectra of an atom are governed by the same set of eigenchannel data. As a result, properties of the discrete spectrum can be deduced from those of the continuum spectrum and vice versa.

In our present case, below the $^2D_{5/2}$ threshold, $4d \rightarrow nf, np$ Rydberg series are actually autoionization resonances because they are imbedded in the continuum of $5s$ and $5p$ electrons. However, as the perturbation from outer electrons are weak, these Rydberg series are not affected much by the background continuum. In Fig. 6, one sees that the eigenamplitudes of Xe below the $4d$ thresholds are small. In particular, those associated with the $4d \rightarrow f$

TABLE II. The *jj-LS* transformation matrix.

		d^9f			d^9p		
	j-j'	^3P	^3D	^1P	^3D	^3P	^1P
$d \rightarrow f$	$\frac{5}{2}$-$\frac{7}{2}$	−0.535	−0.378	0.756	0	0	0
	$\frac{5}{2}$-$\frac{5}{2}$	0.717	−0.676	0.169	0	0	0
	$\frac{3}{2}$-$\frac{5}{2}$	0.447	0.632	0.632	0	0	0
$d \rightarrow p$	$\frac{5}{2}$-$\frac{3}{2}$	0	0	0	−0.316	0.548	0.775
	$\frac{3}{2}$-$\frac{3}{2}$	0	0	0	0.632	0.730	−0.258
	$\frac{3}{2}$-$\frac{1}{2}$	0	0	0	0.707	−0.408	0.577

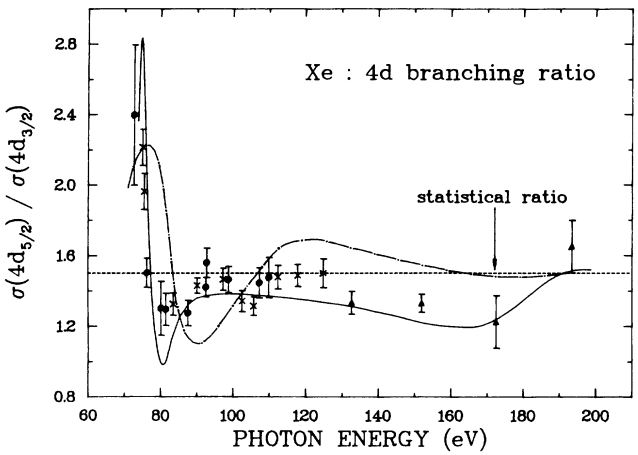

FIG. 7. Comparison between theory and experiment on the $4d_{5/2}$ to $4d_{3/2}$ branching ratio for Xe. Experiment: Adam *et al.*, Ref. 25; Shannon *et al.*, Ref. 26; Banna *et al.*, Ref. 27. Theory: ——, RRPA, this work (note that the RRPA results in Ref. 22 are different from the ones here near the thresholds because of a slight numerical problem there); —·—, DF results of Ong and Manson, Ref. 24.

channels nearly vanish. This is consistent with the observed spectrum of Xe shown in Fig. 2, where the *np* resonance lines are weak, and where the *nf* series hardly show up at all. Along the isoelectronic sequence, it is obvious from Fig. 6 that the $4d \rightarrow f\ ^1P$ amplitudes of the stripped ions are no longer suppressed by the potential barrier right below the ionization thresholds. Thus we expect that there should be strong resonance lines arising from the $4d^9nf\ ^1P$ series in Cs^+, Ba^{2+}, and La^{3+}. Furthermore, judging from the eigenamplitudes of Xe, these lines should be the strongest in Ba^{2+}, as the discrete excitation region of the Ba^{2+} spectrum is right where the $4d \rightarrow f\ ^1P$ amplitude peaks. The appearance of strong resonance lines in the observed Ba^{2+} spectrum shown in Fig. 2 certainly supports this speculation. More detailed discussion of the discrete spectra for Xe-like ions can be found in Ref. 8.

While quantitative studies of these resonances would require the inclusion of the 5*s* and 5*p* excitation channels, the effect of channel interactions on autoionization resonances can be studied in the region between the $^2D_{5/2}$ and $^2D_{3/2}$ thresholds. There, the $4d_{5/2} \rightarrow p_{3/2}, f_{5/2}, f_{7/2}$ channels become open, while the $4d_{3/2} \rightarrow p_{1/2}, p_{3/2}, f_{5/2}$ channels remain closed. As a result, only the latter three series autoionize between the two thresholds and for convenience, they are labeled as np', $n\bar{p}'$, and nf' resonances. The interesting thing here is that the profiles of those resonances are determined mainly by correlations between the open and the closed 4*d* excitation channels rather than by couplings with the 5*s* and 5*p* background continuum. The situation is similar to the Beutler-Fano resonances[28] in rare-gas atoms between the $^2P_{3/2}$ and $^2P_{1/2}$ thresholds where the $np_{1/2} \rightarrow n's_{1/2}, n'd_{3/2}$ Rydberg series are imbedded in the $np_{3/2}$ continuum. *Ab initio* studies of the Beutler-Fano resonances have been carried out recently with success using a technique that utilizes MQDT in analyzing RRPA eigenchannel data.[29] The same technique is employed here to study the autoionization resonances between the two 4*d* thresholds.

Results on the resonance profiles are shown in Fig. 8 as functions of the effective quantum number ν defined by the Rydberg formula as $\omega = I_{3/2} - Z_c^2/2\nu^2$, with $I_{3/2}$ being the energy of the $^2D_{3/2}$ threshold, and Z_c being the effective core charge. By plotting the resonances in this way, they are almost periodic functions of ν along the Rydberg series so that it is sufficient to study only portions of them. In Fig. 8, one sees that there are two np' series and one nf' series in these spectra. Except for the shift in the resonance positions, the two np' series remain very much the same along the isoelectronic sequence. The nf' resonances, on the other hand, change drastically with increasing *Z*. In Xe, these nf' resonances are extremely sharp. In Cs^+ and Ba^{2+}, they suddenly become very broad and very strong, and in La^{3+}, they start to weaken again.

The change in the oscillator strengths of these resonances (the total area under them) with increasing *Z* are consistent with the change in the threshold values of the $4d \rightarrow f\ ^1P$ amplitudes of these Xe-like ions shown in Fig. 6. Indeed, the nf' resonances are the strongest in Ba^{2+} as we have speculated earlier. Furthermore, as the width of a resonance is determined by the strength of interactions between the closed and the open channels,[30] the profiles of these nf' resonances reflect the changing correlation effects among the $4d \rightarrow f$ channels near the thresholds of these Xe-like ions.

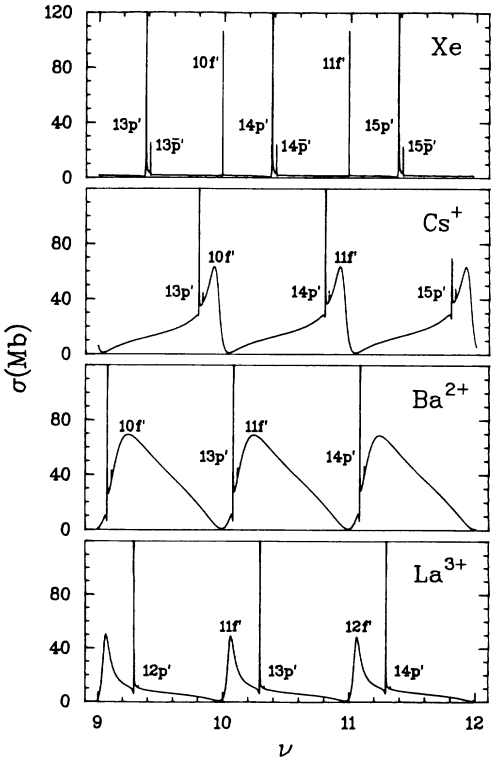

FIG. 8. Autoionization resonances between the $^2D_{5/2}$ and $^2D_{3/2}$ thresholds of Xe, Cs^+, Ba^{2+}, and La^{3+} as functions of the effective quantum number ν.

IV. $4f$ ORBITAL COLLAPSE

We show in the previous section systematic trends in the photoionization of inner $4d$ shells for Xe-like ions. In particular, we find that changes in the spectra along the isoelectronic sequence can be understood in terms of changes in the Xe spectrum as photon energy increases. From the eigenchannel data, we find that the $4d \rightarrow f$ channels are not interacting strongly with the $4d \rightarrow p$ ones, and that the former channels are strongly term dependent, but not the latter ones. Also, there is a gradual change in correlation effects among the $4d \rightarrow f$ channels leading to a shift in coupling schemes as energy increases and to drastic changes in the nf' resonances profiles along the isoelectronic sequence. Since these spectra are determined mainly by the $4d \rightarrow f$ channels and are not affected much by outer valence electrons, similar features should exist in the photoionization of the nd shells for other closed-shell systems. Indeed, photoionization cross sections of group-IIB elements Zn, Cd, and Hg,[31] as well as that of Pd,[32] all have strong peaks above the ^2D thresholds just like that of Xe shown in Fig. 2. Furthermore, branching ratios and angular distribution asymmetry parameters of these atoms all resemble corresponding Xe data shown in Figs. 3 and 4. We thus expect that the systematic trends found here should be applicable to the isoelectronic sequences of these atoms also.

There is, however, a rather special feature in the photoionization for Xe-like ions, namely, the collapse of the $4f$ orbital along the Xe isoelectronic sequence. As we have pointed out in Fig. 5 before, the eigenquantum defects μ_α of the $4d \rightarrow f$ channels increase rapidly by one above the $4d$ thresholds of Xe. Corresponding eigenphase shifts $\delta_\alpha = \pi\mu_\alpha$ thus go through changes of π in this region. Similar observation has been made by Manson and Cooper[14] in a Herman-Skillman potential calculation where the phase shifts of the continuum f wave functions increase by π in passing through shape resonances arising from the inner well of the effective potential. From the Xe data shown in Fig. 2, it is obvious that potential results are substantially modified by electron correlations. Nevertheless, if one simulates the correlated results by some model potential calculations, one can then interpret the behavior of μ_α as an indication of the existence of shape resonances in these potentials. Furthermore, the fact that the three μ_α of the $4d \rightarrow f$ channels are so different in Fig. 5 suggests that the model potentials associated with these channels are strongly term dependent. Indeed, from the rates of change of μ_α in going through increases of one, the shape resonance of the ^1P potential must be very broad, while those of the ^3P and ^3D potentials must be much narrower. This is consistent with the widths of the resonance peaks in the eigenamplitudes of the $4d \rightarrow f$ ^1P, ^3P, and ^3D channels for Xe shown in Fig. 6.

These shape resonances exist because of the barrier in the effective potential which separates the inner well from the outer one. They are actually eigenstates of the inner well which can "autoionize" by tunneling out of the potential barrier. When an f wave function passes through one of these shape resonances, its amplitude inside the barrier is enhanced. As energy increases further, the amplitude goes back to its normal size, but in the process, the first node of this wave function moves from the outer well into the inner one, and the corresponding phase shift increases by π.[14] The most interesting thing is that along the isoelectronic sequence, the inner well becomes deeper and deeper as Z increases.[8] As a result, these shape resonances gradually move below the $4d$ thresholds, interact with the $4d^9nf$ Rydberg series which are hydrogenlike eigenstates of the outer well, and eventually become the lowest bound states of the corresponding model potentials.

The lowering of shape resonances into the discrete excitation region of the spectrum was pointed out by Goeppert Mayer[33] in explaining the collapse of the $4f$ orbital. From the above discussion, it is obvious that the quantum defects of the entire $4d^9nf$ Rydberg series must increase by about one in the process. Furthermore, from the systematic trend of μ_α shown in Fig. 5, it appears that the $4f$ orbital is collapsed at a much faster rate in the triplet states than in the singlet state. Thus in quantitative discussions of the collapse phenomenon, the term dependence of the $4f$ orbital should be taken into account. In Fig. 5 it also appears that in Ba^{2+} the $4f$ orbital is collapsed in the $4d^9 4f\ ^3P, ^3D$ states, but is not quite collapsed in the ^1P one. These observations are indeed verified by a recent term-dependent HF calculation of Cheng and Froese Fischer[8] where more detailed discussions of the collapse phenomenon in Xe-like ions can be found.

Finally, we should mention that in Fig. 8, the "flipping" of the nf' resonance profiles from Cs^+ to Ba^{2+} clearly demonstrates the lowering of the ^1P shape resonance from above the thresholds in Cs^+ to below in Ba^{2+}, thereby altering the locations and profiles of the nf' resonances in the process. If these resonances can be resolved experimentally, they may provide the best information on the dynamics of electron correlations and the orbital collapse phenomenon.

ACKNOWLEDGMENTS

The authors would like to thank Dr. T. B. Lucatorto and Professor H. P. Kelly for communicating their results, and Dr. V. Radojević for technical assistance. The work of K. T. Cheng is supported by the U. S. Department of Energy, Office of Basic Energy Sciences under Contract No. W-31-109-ENG-38. The work of W. R. Johnson is supported in part by the National Science Foundation, Grant No. PHY-81-07382.

[1] R. Haensel, G. Keitel, P. Schreiber, and C. Kunz, Phys. Rev. 188, 1375 (1969).
[2] J. W. Cooper, Phys. Rev. Lett. 13, 762 (1964).
[3] T. B. Lucatorto, T. J. McIlrath, J. Sugar, and S. M. Younger, Phys. Rev. Lett. 47, 1124 (1981).
[4] J. L. Dehmer, A. F. Starace, U. Fano, J. Sugar, and J. W. Cooper, Phys. Rev. Lett. 26, 1521 (1971).
[5] G. Wendin and A. F. Starace, J. Phys. B 11, 4119 (1978).

[6]J. P. Connerade and M. W. D. Mansfield, Phys. Rev. Lett. 48, 131 (1982).
[7]J. E. Hansen, A. W. Fliflet, and H. P. Kelly, J. Phys. B 8, L127 (1975).
[8]K. T. Cheng and C. Froese Fischer, Phys. Rev. A 28, 2811 (1983), preceding paper.
[9]W. R. Johnson and C. D. Lin, Phys. Rev. A 20, 964 (1979).
[10]W. R. Johnson and K. T. Cheng, Phys. Rev. A 20, 978 (1979).
[11]M. J. Seaton, J. Phys. B 11, 4067 (1978), and references therein.
[12]U. Fano, J. Opt. Soc. Am. 65, 979 (1975), and references therein.
[13]C. M. Lee and W. R. Johnson, Phys. Rev. A 22, 979 (1980).
[14]S. T. Manson and J. W. Cooper, Phys. Rev. 165, 126 (1968).
[15]A. F. Starace, Phys. Rev. A 2, 118 (1970).
[16]D. J. Kennedy and S. T. Manson, Phys. Rev. A 5, 227 (1972).
[17]M. Ya. Amusia and N. A. Cherepkov, Case Stud. At. Phys. 5, 47 (1975).
[18]H. P. Kelly, S. L. Carter, and B. E. Norum, Phys. Rev. A 25, 2052 (1982).
[19]T. C. Chiang, D. E. Eastman, F. J. Himpsel, G. Kaindl, and M. Aono, Phys. Rev. Lett. 45, 1846 (1980).
[20]A. Msezane, R. F. Reilman, S. T. Manson, J. R. Swanson, and L. Armstrong, Jr., Phys. Rev. A 15, 668 (1977).
[21]K. N. Huang, W. R. Johnson, and K. T. Cheng, At. Data Nucl. Data Tables 26, 33 (1981).
[22]W. R. Johnson and V. Radojević, J. Phys. B 11, L773 (1978).
[23]S. H. Southworth, P. H. Kobrin, C. M. Truesdale, D. Lindle, S. Owaki, and D. A. Shirley, Phys. Rev. A 24, 2257 (1981).
[24]W. Ong and S. T. Manson (unpublished, results obtained from Ref. 23).
[25]M. Y. Adam, F. Wuilleumier, S. Krummacher, N. Sandner, V. Schmidt, and W. Mehlhorn, J. Electron Spectrosc. Relat. Phenom. 15, 211 (1979).
[26]S. P. Shannon, K. Codling, and J. B. West, J. Phys. B 10, 825 (1977).
[27]M. S. Banna, M. O. Krause, and F. Wuilleumier, J. Phys. B 12, L125 (1979).
[28]H. Beutler, Z. Phys. 93, 177 (1935); U. Fano, Nuovo Cimento 12, 154 (1935).
[29]W. R. Johnson, K. T. Cheng, K. N. Huang, and M. LeDourneuf, Phys. Rev. A 22, 989 (1980).
[30]U. Fano, Phys. Rev. 124, 1866 (1961).
[31]W. R. Johnson, V. Radojević, P. Deshmukh, and K. T. Cheng, Phys. Rev. A 25, 337 (1982).
[32]V. Radojević and W. R. Johnson, J. Phys. B 16, 177 (1983).
[33]M. Geoppert Mayer, Phys. Rev. 60, 184 (1941).